ACS APPLIED MATERIALS & INTERFACES

www.acsami.org
Research Article

Achieving High-Temperature Stable Structural Color through Nanostructuring in Polymer-Derived Ceramics

Benedikt F. Winhard, Alberto Gomez-Gomez, Laura G. Maragno, Diego Ribas Gomes, and Kaline P. Furlan*

Cite This: ACS Appl. Mater. Interfaces 2024, 16, 22379−22390
Read Online

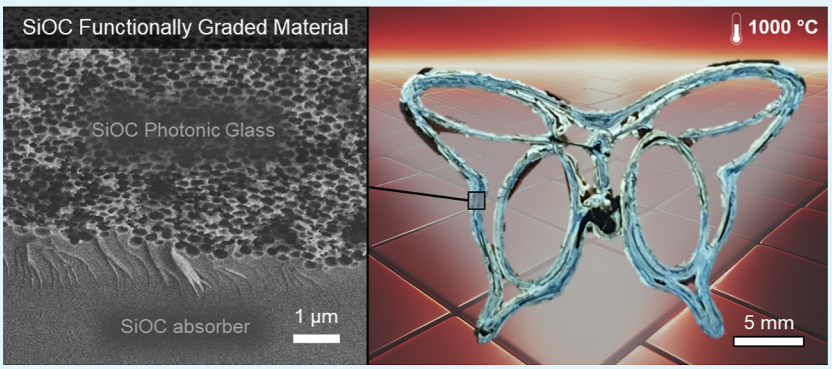

ABSTRACT: Structural colors offer a myriad of advantages over conventional pigment-based colors, which often rely on toxic chemical substances that are prone to UV degradation. To take advantage of these benefits in demanding environments, there is growing interest in producing structural colors from ceramics. Polymer-derived ceramics (PDCs) emerge as a compelling choice, presenting two distinct advantages: their enhanced shape ability in their polymeric state associated with impressive temperature resistance once converted to ceramics. This study pioneers the fabrication of noniridescent structural colors from silicon oxycarbide (SiOC) PDC, enabled by the nanostructuring of an inverse photonic glass within the PDC material. This design, a functionally graded material with an inverse photonic glass (FGM-PhG) structure, leverages the innate light-absorbing properties of SiOC, yielding a vivid structural color that maintains its saturation even in white surroundings. This study elucidates the process−structure−properties relationship for the obtained structural colors by investigating each layer of the functionally graded material (FGM) in a stepwise coating deposition process. To further emphasize the exceptional processing flexibility of PDCs, the three-step process is later transferred to an additive manufacturing approach. Finally, the FGM-PhG structural colors are demonstrated to have remarkable thermal stability up to 1000 °C for 100 h, possibly making them the most thermally stable ceramic structural colors to date.

KEYWORDS: *structural color, polymer-derived ceramics, colloids, self-assembly, additive manufacturing*

INTRODUCTION

Structural coloration, a unique phenomenon observed in nature, relies on the manipulation of light by micro and nanostructured materials rather than the use of pigments or dyes to produce color.[1,2] The inherent benefits of this strategy include superior color longevity, resilience to UV degradation, and resistance to chemical degradation, all of which are not commonly found in traditional pigment-based coloration, which in addition are often made from toxic chemical substances.[2,3] These advantageous properties of structural colors can be further amplified when they are produced with ceramic materials. Ceramics, owing to their excellent thermal and chemical stability, can potentially enable structural colors to be used under challenging environmental conditions such as high UV radiation, corrosive environments, and even high temperatures.[4−6] Thus, the incorporation of structural coloration strategies into ceramics heralds a new era for durable, vibrant, and environmentally stable coloration systems, expanding their applicability to demanding surroundings.

A few studies have demonstrated the production of structural colors based on three-dimensional (3D) ceramic photonic structures that could potentially be used in harsh

Received: January 22, 2024
Revised: March 12, 2024
Accepted: March 13, 2024
Published: April 18, 2024

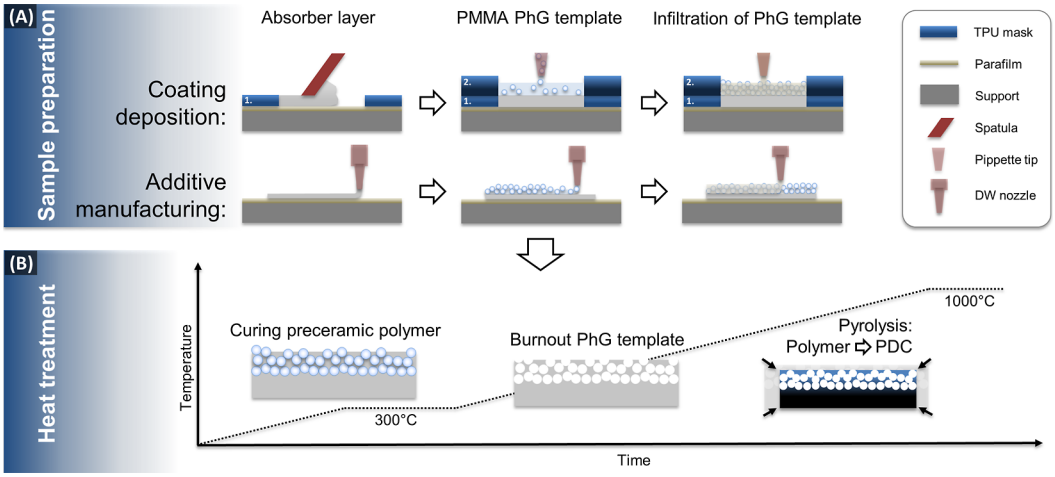

Figure 1. (A) Processing scheme for FGM-PhG samples produced in this study: samples were prepared either by a three step coating deposition (doctor blading, drop casting, and infiltration) or by a three step AM process (print the dense absorber layer, print the PhG template, and print infiltration material). (B) Obtained samples were heat-treated in a three step cycle comprising preceramic polymer curing, PhG template removal, and conversion to ceramic-based photonic structure via pyrolysis.

environments.[7,8] However, fabricating such structures traditionally, i.e., with ceramic particles as starting material, can bring limitations in design complexity and limits applicable shaping methods.[9] Alternatively, it has been shown that such structures can also be produced by utilizing preceramic precursors.[10−15] Here, preceramic polymers are prominent starting materials. They facilitate macroscale shaping, thereby enabling the fabrication of structures via additive manufacturing (AM), which overcomes potential processing barriers with conventional ceramic processing strategies.[16] Although several research groups have already applied AM to produce complex ceramic structures from preceramic polymers,[17,18] the investigation of AM of structural colors using preceramic polymers remains unexplored. Instead, other strategies to print structural colors have been studied, but they were often polymer based, thus lacking UV resistance and being prone to deformation under moderate temperatures.[19,20] Meanwhile, the AM of ceramic-based spherical particles requires the incorporation of large amounts of template particles in a binder system and may lack mechanical integrity, when consisting of loose ceramic particles.[21,22]

Regardless of the shaping method, the application as structural color requires that the structure contains features' sizes with a narrow variation and in the range of the wavelength of interest, i.e., nanometer to sub-micrometer, precisely distributed in the 3D macroscale. A study by Zhou et al.[23] demonstrated the possibility to generate ceramic-based photonic structures utilizing preceramic polymers as starting material and performing subsequent pyrolysis to form polymer-derived porous ceramics. Their porous PDC had a photonic crystal (PhC) structure and, thus, presented an angle dependent structural coloration. The iridescence of PhCs stems from their long-range ordered structure. In contrast, a photonic glass (PhG) structure demonstrates a disordered arrangement with only short-range order, leading to angle-independent structural colors.[24,25] This characteristic is beneficial in applications such as displays or sensors, where the color should appear the same no matter the viewing angle or when locking a precise viewing angle is not feasible, respectively.

In previously reported studies, carbon is usually added as an absorber between ceramic particles to maintain the saturation of the structural color in front of white backgrounds, too. However, this limits the structures' temperature stability under ambient conditions (air) to ∼350 °C due to carbon burnout.[26] Meanwhile, preceramic polymers not only present outstanding shaping abilities, but the later conversion to ceramic glass results in excellent thermal stability, making them ideal for use in harsh environments.[16,27]

In this study, we investigated an approach to produce ceramic-based PhG having preceramic precursors as starting material, which enabled the printing of ceramic structural color that demonstrates high color saturation even under diffuse illumination and white surroundings. This is made possible by producing a functionally graded material (FGM) through the integration of a bulk absorber layer underneath the photonic structure. The resulting FGM-PhG forms a mechanically robust and highly temperature-stable saturated structural color that is particularly advantageous for applications in harsh environments. First, this study introduces the nonintuitive concept of FGM-PhG structural color made of SiOC, a ceramic material, which is light absorbing, thus appearing black in its bulk form. Subsequently, the process−structure−properties relationship is explored for FGM-PhG samples produced with a three-step coating process (Figure 1). Later, the transition of the coating process into an AM process is showcased, demonstrating the exceptional processing flexibility for structural colors made of PDCs. Lastly, the thermal stability of the FGM-PhG structural colors is examined. The results show that using PDCs can enhance the thermal stability of ceramic structural colors while benefiting from the ease of processing associated with polymers. This pioneering strategy opens up new possibilities for the fabrication of noniridescent SiOC ceramic structural colors, potentially broadening the applicability of structural colors in harsh or demanding environments.

RESULTS AND DISCUSSION

In the earlier study by Zhou et al.,[23] custom-made preceramic polymers were used to infiltrate photonic crystals' templates. The resulting silicon carbide inverse opal samples presented

https://doi.org/10.1021/acsami.4c01047
ACS Appl. Mater. Interfaces 2024, 16, 22379−22390

structural coloration; however, iridescent structural coloration, i.e., color, changes depending on the radiation incident (or viewing) angle. In this work, we aimed to develop non-iridescent structural colors and, therefore, focused on fabricating PhG structures. The commercially available MK-precursor was utilized, which can be processed under ambient conditions. In "bulk", i.e., as a nonporous sample, it forms SiOC during pyrolysis.[28,29]

The as-delivered poly(methyl methacrylate) (PMMA) dispersions that serve as templates for the PhG structure contain water as a dispersion medium. This brings hurdles to our described FGM strategy (Figure 1A) since the PDC layer presents a hydrophobic character. Moreover, deposition of aqueous PMMA dispersions resulted in the formation of PhCs, leading to inverse SiOC PhCs with iridescent structural coloration, as can be seen in the scanning electron microscopy (SEM) cross sections and photographs taken at different observation angles (Figure 2A). Blue, turquoise, and green

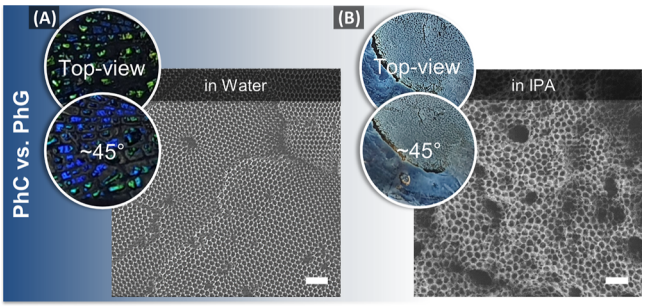

Figure 2. Photographs taken from top-view and at ~45° observation angle, alongside the corresponding SEM cross sections, of FGM samples produced with a PMMA dispersion in either (A) water or (B) IPA. Scale bars: 1 μm.

colors formed in the PhC samples with a clear dependence on the angle of observation. To address the challenge of transitioning from ordered to disordered particle arrangements, various strategies have been investigated: the adjustment of the surface charge of substrates to alter particle mobility,[30] the addition of salts to colloids to destabilize them through increased ionic concentration, which screens electrostatic repulsion among particles,[24,25,31] or via heteroaggregation, which introduces a mix of particles with different surface charges, leading to aggregate formation and sedimentation of disordered deposits.[32]

To tackle both challenges, i.e., the prevention of long-range order and improved substrate wettability, we considered the adaptation of the dispersion medium. Knowing that some organic media present lower surface tension than water and that there is a basic relation between surface tension and wettability, we have selected the organic medium isopropyl alcohol (IPA) to redisperse PMMA particles (refer to Methods for details). As expected, the contact angle of water-based and IPA-based PMMA dispersions on the PDC absorber layer differed greatly, achieving values of 108 ± 4° and <10°, respectively (Figure S1). Not only could the wetting be controlled by the selection of the dispersion medium, but it could also direct the colloidal assembly (Figure 2).

While water-based PMMA dispersions formed PhC templates, IPA-based dispersions led to the desired PhG template structure with noniridescent structural coloration. To investigate the possible reasons for such a difference, the zeta-potential of the dispersions was assessed, resulting in values of −35.6 ± 0.7 and −33.4 ± 0.9 mV at pH values of 6.5 and 8.7 for IPA- and water-based dispersions, respectively. Since both dispersions presented similar values with corresponding similar good dispersion stability (i.e., no sedimentation was visible), the potential colloidal destabilization in IPA, which would lead to particle aggregation and thus formation of PhG templates,[32] was excluded as a cause for the formation of amorphous PMMA-templates. Thereby, we associate the observed differences with the dispersion medium characteristics, namely, surface tension and wettability. The former accounts to 22 and 72 mN m^{-1} for IPA and water (at 20 °C), respectively, thus about three times larger for water than IPA.[33] During dispersion medium evaporation in colloids, capillary forces help on attracting particles contributing to the formation of ordered assemblies.[34] As the capillary force is directly proportional to the surface tension, water-based dispersions present higher capillary forces, and the capillary forces exerted between particles in IPA seem to be too small to form long-range order. Moreover, low wetting led to a continuously receding contact line for aqueous dispersions during drying, which can additionally support crystallization of colloids as previously reported.[35,36]

Following the goal of generating noniridescent structural colors, the following sections focused on investigating the process−structure−property relationships and the application of such in an FGM concept. In the absence of previous studies that investigated the optical properties of MK-based 3D photonic structures, the following investigation of this study focused on characterizing the optical properties and color appearance of the 3D photonic structures in comparison to MK-based "bulk" layers.

Generation of Color by 3D FGM Structuring of a Black Material. The formation of SiOC from the polymeric preceramic precursor MK during pyrolysis in a nitrogen atmosphere was reported before,[28,29] and the energy dispersive X-ray spectroscopy (EDX) analysis of pyrolyzed samples confirmed the presence of Si, O, and C, while the X-ray diffraction (XRD) analysis corroborated the expected presence of an amorphous phase (see Supporting Information, Figure S2). The derivative thermogravimetry (DTG) of a MK-infiltrated photonic structure containing both MK and PMMA did not show additional decomposition steps but presented all decomposition steps that could also be found in the DTG analyses of each individual component (Figure 3A): from 150 to 250 °C, decomposition of weak head-to-head bonds in PMMA was observed, as previously reported.[37,38] The decomposition in the temperature range of 200−300 °C could be addressed to the release of water and ethanol in MK,[39] as well as the decomposition of unsaturated chain ends in PMMA.[37,38] At 380 °C, a significant peak marked by random scission of the polymer chains in PMMA occurred, leading to decomposition into its monomer, methyl methacrylate.[40] At around 570 °C, the DTG further reveals the release of methane from MK.[39] Finally, MK displayed decomposition at 750 °C, which can be attributed to the release of methane, hydrogen, and ethane.[39] Each decomposition step found in the "MK and PMMA" sample corresponded to a decomposition step in either of the two individual components, thus implying no additional chemical interaction between the two components during pyrolysis. Hence, the SiOC formed in the 3D porous photonic structures

https://doi.org/10.1021/acsami.4c01047
ACS Appl. Mater. Interfaces 2024, 16, 22379−22390

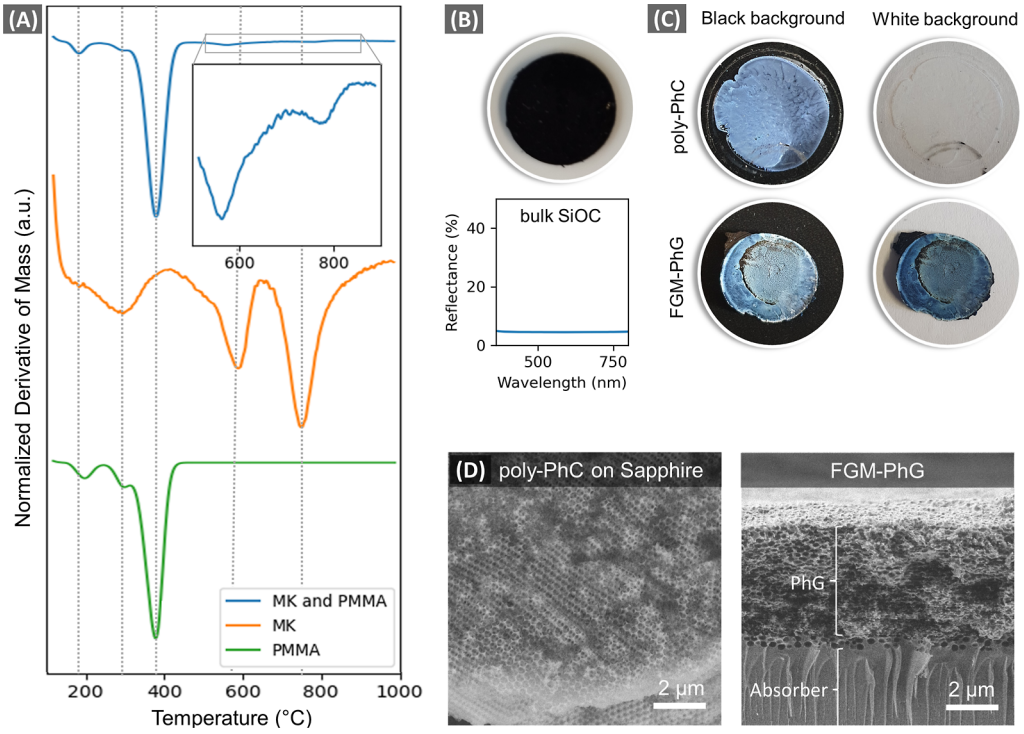

Figure 3. (A) DTG curves for PMMA, MK, and a MK-infiltrated PhG containing both materials. (B) Photograph of a bulk SiOC sample and its corresponding reflectance spectrum. (C) Photographs of a poly-PhC sample produced on sapphire and an FGM-PhG sample, both captured against black and white backgrounds. (D) SEM cross sections of a poly-PhC sample produced on sapphire and of an FGM-PhG sample.

were considered not to differ from the composition of a bulk sample.

SiOC—also known as black glass[16,27]—contains sp^2-hybridized carbon, which absorbs electromagnetic waves in the entire visible wavelength range.[16] This usually leads to a black appearance and low reflectance for bulk samples (Figure 3B), which at first may seem to potentially hinder the formation of structural coloration if the absorption component is greater than the 3D structurally originated reflectance. Hence, to examine whether structural color can also be formed with SiOC, only the "inverse" PhG structures, i.e., structures generated after burn-out and pyrolysis but without the underlying bulk SiOC-layer were analyzed and compared with FGM-PhGs. As shown in Figure 3C, a vivid blue structural color can indeed be achieved in 3D MK-based photonic structures. It is clear that scattering dominates the absorption of light in this sample due to the introduction of many material−air interfaces with the inverse polycrystalline photonic crystal (poly-PhC) structure (Figure 3D). Additionally, pores reduce the absorbance in poly-PhC samples due to the replacement of the volume fraction of absorbing SiOC with air, thus reducing the fraction of SiOC that light must interact when traveling through the sample.

When the poly-PhC sample is placed in front of a white background, no hue is visible, and the photonic structure appears completely white (Figure 3C) because the light that passes through the photonic structure gets reflected back from the white background, thus overlaying with the selective reflection from the poly-PhC (Figure 4A). This additionally demonstrates the low absorbance of the 3D photonic structure even when made out of SiOC, while also showing that the previous blue hue visible in front of a black background, originates from selective reflectance. The "absence" of color for photonic structures in front of highly reflecting backgrounds is a commonly observed phenomenon, which hampers their applicability in such surroundings. Moreover, white surroundings and diffuse illumination can also lead to loss of color saturation.[19,20,41] To improve the color saturation, i.e., to reduce incoherent scattering, usually an external background is added below the photonic structure (i.e., the structure is placed on top of a black surface) or nanoparticles are added within the structure.[2,7,8,21,26,32,42−46] In this study, however, the highly absorbing SiOC material that is already being used to form 3D photonic structures can additionally be utilized to remove incoherent scattering via nonselective absorption. Hence, to absorb the transmitted light, an FGM was fabricated that consisted of a PhG structure on top of an absorbing bulk SiOC-layer (Figure 3D). The additional bulk SiOC-layer absorbed the transmitted light effectively such that blue structural coloration was visible even in front of a white background and highly illuminated surroundings (Figure 3D). It is important to note that this new FGM-PhG concept uses exactly the same material for the PhG as well as the absorber layer, and that the selective reflectance and, thus, structural coloring, arises due to the material structuring in 3D. Further, this concept offers another advantage as it "removes" the additional interface that would be present in case of two different materials, preventing potential additional scattering events at the PhG-absorber interface.[2] Moreover, in the chromaticity diagram, the position of the FGM-PhG sample is closer to the perimeter than the position of the poly-PhC sample, which indicates a higher color saturation for the FGM-PhG sample (Figure 4B). We associate this increased color saturation to the matching interface in the FGM-PhG, which reduces potential incoherent scattering.

https://doi.org/10.1021/acsami.4c01047
ACS Appl. Mater. Interfaces 2024, 16, 22379−22390

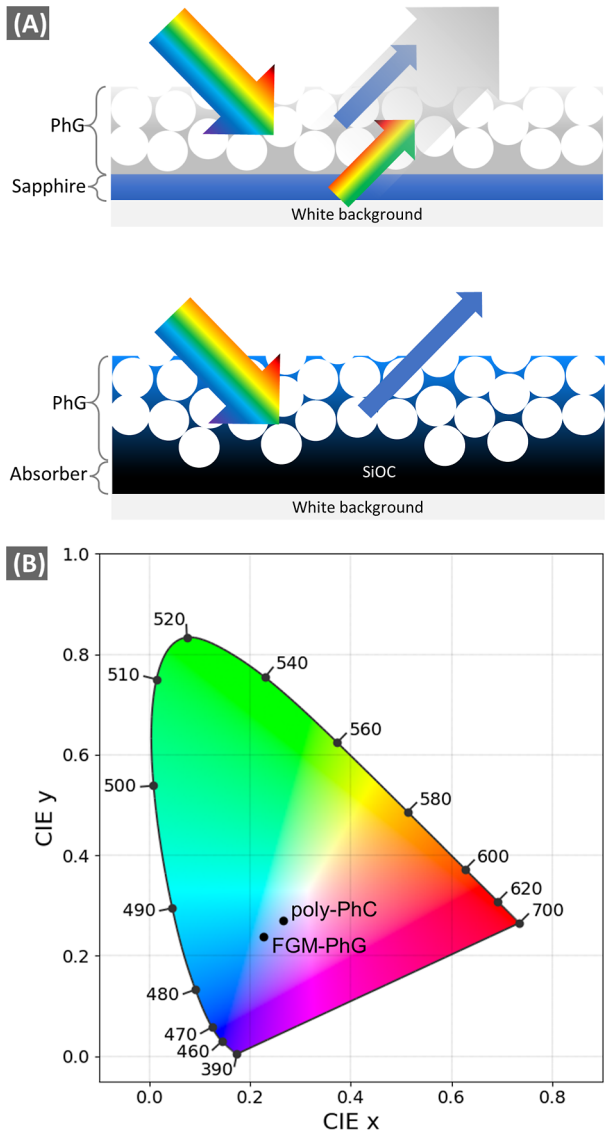

Figure 4. (A) Schematic representations of the interaction of light with poly-PhC on sapphire (top) and the FGM-PhG sample (bottom). (B) Segment of the chromaticity diagram illustrating positions of the poly-PhC sample as well as the FGM-PhG sample.

Investigation of Process–Structure–Property Relationships. In order to further improve the color quality, the process–structure–properties relationship was studied in detail in order to derive design requirements for later transfer into the AM process. In a first parameter study, the particle template size was varied to potentially generate structural colors other than blue. Due to the associated shrinkage during preceramic polymer conversion and pyrolysis, PMMA-template particles with a diameter of 286 nm resulted in an average pore size of 186 nm, and particles with 406 and 499 nm formed pores with 291 and 361 nm, respectively (Supporting Information, Figure S3).

When increasing the particle template size from 286 to 406 nm, the blue hue became brighter and shifted toward turquoise coloration in both poly-PhC and FGM-PhG samples (Figure 5A). This agrees with the corresponding reflectance spectra for samples produced with 406 nm template particles, which are shifted toward higher wavelengths in comparison to spectra for the 286 nm template size (Figure 5B). The shift of reflectance toward higher wavelengths with increasing pore—or generally speaking feature size—is a commonly observed phenomenon for photonic structures.[2,47−50] In photonic structures, light scattering can be distinguished between two different processes: scattering from individual features (e.g., particles or pores) and coherent scattering caused by interference of scattered light from features in the photonic structure.[2,49] While the single feature resonances scale with the optical diameter following $n_{pp}d_p$ (where n_{pp} is the refractive index of the particles/pores and d_p is the particle or pore diameter), the characteristic scale for coherent scattering is the effective center-to-center distance D_{cc} of the features following $n_{eff}D_{cc}$. For a close packed photonic structure (as the ones produced in this study), both characteristic scales' sizes increase with template size; hence, the overall reflectance shifts toward higher wavelengths. Therefore, an increase of the PMMA-template size further to 499 nm did not lead to a change in color but rather caused the samples to become whiter. This loss in color with increasing template size is caused by a broad reflectance in the visible wavelength range below a certain threshold wavelength, which is dependent on the initial template particle size. Slight differences in the sample whitening can be seen for the two sample types. While for the poly-PhC a "clear" white appearance is observed for the 499 nm template, the FGM-PhG still presented a slight blue hue, however with significant loss in saturation (Figure 5A). This corroborates the measured differences in the reflectance for both sample types (Figure 5B). Whereas FGM-PhG samples demonstrated a gradual decline in reflectance with increasing wavelength, the poly-PhC samples' reflectance first decreased but increased again forming a local maximum at 570 nm before dropping to small reflectance values. The peak found in poly-PhC samples can be attributed to coherent scattering, while the gradual decline found in both samples can be assigned to single feature (pore) resonances.[49] Hence, in the FGM-PhG single feature resonances dominate, whereas in the poly-PhC additional coherent scattering by the crystalline domains is observed. The peak formed by coherent scattering in poly-PhC samples theoretically allows one to form other structural colors than blue; however, as the single feature resonances were too dominant, this is not possible. The same behavior was previously observed by Magkiriadou et al.[49] for PhGs made of PMMA particles.

To be able to generate other structural colors in the poly-PhC samples, resonances from single features must be reduced concomitantly with the maintenance of coherent scattering. To shift scattering events to a different wavelength range, one might contemplate adjusting the effective refractive index n_{eff} of the photonic structure by altering the refractive index of the SiOC material n_{SiOC}. It has been demonstrated that the refractive index of SiOC can vary within the range for refractive indices associated with silica and silicon carbide (between 1.5 and almost 2.7), depending on the material's content of oxygen and carbon.[51] However, it is crucial to note that alterations made to the refractive index of SiOC would impact both single feature resonances and coherent scattering simultaneously, causing both scattering events to shift toward either higher or smaller wavelengths. Consequently, such adjustments were not explored in the scope of this study.

As mentioned before, single feature resonances scale with the optical diameter, whereas coherent scattering scales with feature distance. Therefore, to reduce the single feature resonances in the visible, it is necessary to shift them to the

https://doi.org/10.1021/acsami.4c01047
ACS Appl. Mater. Interfaces 2024, 16, 22379−22390

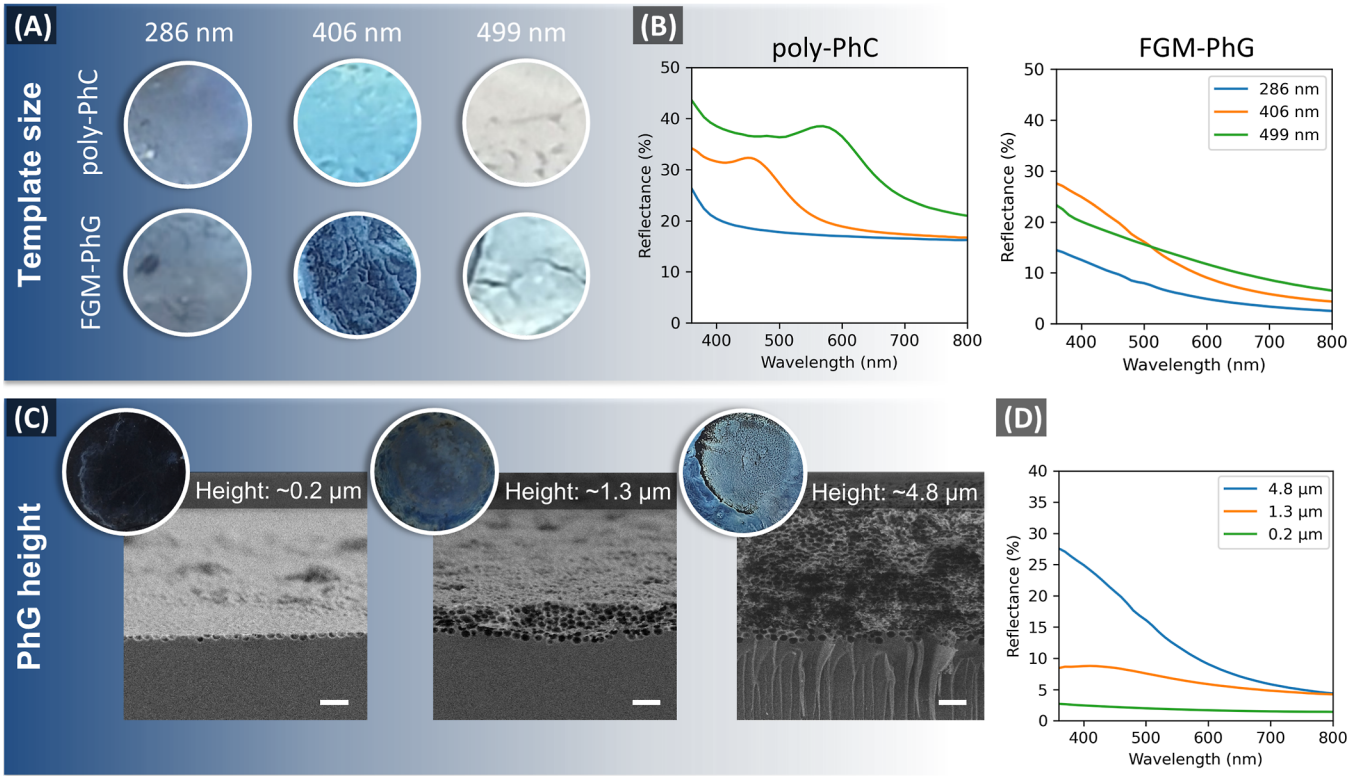

Figure 5. (A) Photographs of poly-PhC samples and FGM-PhG samples produced with different PMMA-template sizes (286, 406, and 499 nm). (B) Reflectance spectra corresponding to all the samples displayed in (A). (C) Photographs and associated SEM cross sections of FGM-PhG samples with various sample heights. Scale bars: 1 μm. (D) Reflectance spectra corresponding to all the samples exhibited in (C).

UV range by—for example—decreasing the pore size, however without altering the effective center-to-center distance D_{cc} to preserve the coherent scattering. This might seem as a paradox since it is not possible to perform such alteration without modification of the particles' surfaces with an additional material layer[52] to increase D_{cc} or without modification of the whole processing chain. As a proof of concept, we show that this paradox might be solved by postprocessing modification via atomic layer deposition, discussed in the Supporting Information (Figure S4), but needs a dedicated study to enable tailoring of the colors. Since the primary focus of this study was to demonstrate the fabrication of noniridescent PDC-based structural colors with high color saturation and the transfer of the optimal design concept to an AM process, we hereby describe further process−structure−property relationships focusing on FGM-PhG design and a PMMA-template size of 406 nm.

By adjustment of the amounts and concentrations of the PMMA dispersions and MK solutions, the final PhG layer height after pyrolysis could be varied (Figure 5C), showing an optimized behavior for layer thicknesses around 1 μm. Optimizing the PhG layer height in the produced FGM-PhG samples is a trade-off between homogeneity and color brightness, so that almost no structural color is visible for the thinner PhG layer height of ~0.2 μm. In this sample, the incident radiation is mainly absorbed by the underlaying PDC layer, reducing the reflectance to 3% or less in the visible wavelength range (Figure 5D). The sample with ~1.3 μm of PhG layer height was crack-free at the macroscale; however, the reflectance in the visible wavelength range was up to three times lower than for the sample with ~4.8 μm height (max. 9% vs 28% reflectance, respectively), showing that the brightness scales with PhG layer height, as in the study by Häntsch et al.[7] Nonetheless, the thicker sample presented visible cracks and a less uniform coloration. The cracks were mainly formed at the second step of sample fabrication due to dispersion medium evaporation, i.e., capillary shrinkage cracking, also reported in previous studies.[53,54] Further increasing the thickness to ~13 μm led to a pronounced and abrupt whitening of the samples (Figure S5). Here, not only the increased thickness was the cause for loss in color but also a significant amount of micron sized pores that can be seen in the SEM cross section next to the submicron pores originating from the PMMA-template particles. These additional pores are also present in FGM-PhG samples with smaller thickness, however in a smaller amount. The origin of these pores can be attributed to several reasons: voids could already be observed in SEM cross sections after PMMA particle assembly (Figure S6), but the number of pores in the pyrolyzed sample is too large to be caused only during particle assembly. Additionally, volatile gases formed during heat treatment could potentially have contributed to such large pores. Both MK and PMMA form volatiles; however, such porosity could not be observed in bulk MK samples after the pyrolysis. Thereby, it is concluded that the pores were formed due to the presence of PMMA particles and their burnout.

Additive Manufacturing of FGM-PhG Structural Colors. To emphasize the exceptional processing flexibility of PDCs over traditional ceramics manufactured from particulate ceramic raw materials, the previous three-step coating process was adapted to an AM process. Specifically, direct writing was selected, given its ability to process inks with a broad range of viscosities.[55] The characterization of the inks' rheological properties showed that the MK-absorber ink presented a shear-thinning flow behavior, which is desirable

https://doi.org/10.1021/acsami.4c01047
ACS Appl. Mater. Interfaces 2024, 16, 22379−22390

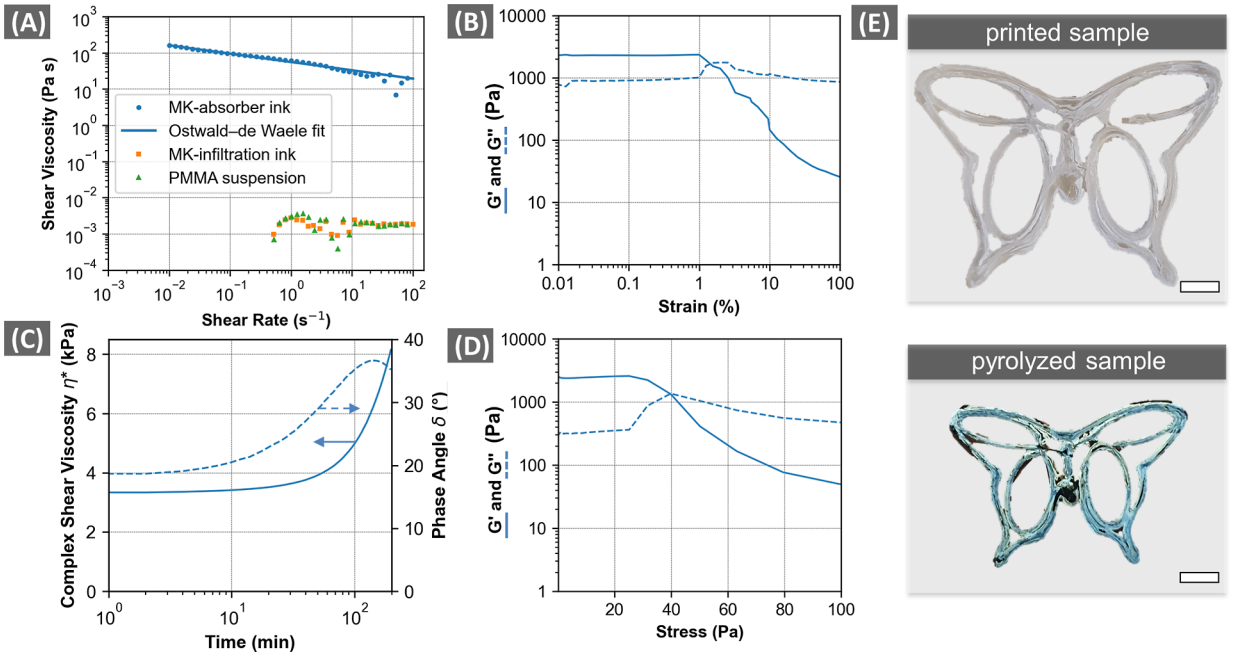

Figure 6. (A) Shear rate ramps of various printing inks. (B) Strain sweep of the MK-absorber ink. (C) Time-resolved curing analysis of the MK-absorber ink. (D) Stress sweep for the MK-absorber ink. (E) Photographs of FGM-PhG butterflies printed with PMMA dispersions of varying concentrations.

for direct writing due to the facilitated extrusion of the ink followed by stability of the printed filament upon removal of load (Figure 6A). The shear-thinning characteristic was additionally confirmed by the flow index n_{fl} = 0.7 (hence, smaller than 1), which was determined by an Ostwald-de Waele fit of the data. In addition to its shear-thinning behavior, the MK-absorber ink also exhibited a linear viscoelastic (LVE) regime up to a strain of 1%, indicating the ink's yield point (Figure 6B) with a corresponding yield stress of approximately 25 Pa (Figure 6D). Additionally, the rheometry measurements also indicated the flow point of the ink at 2% strain and 42 Pa of shear stress. This value assured that the ink could be continuously extruded by our lab-size printer (BioX from CELLINK) with a pressure limit of 200 kPa. Meanwhile, both MK-infiltration ink and PMMA dispersions exhibited very low viscosities, leading to noticeable fluctuations in the measured data, necessitating a reduction in the shear rate interval to 0.5–100 s^{-1}. Neither of these inks demonstrated a significant increase or decrease in viscosity over the measured interval, with both yielding an average viscosity of 1.9 mPa s, suggesting a potential Newtonian fluid behavior, however imprecise taking into account the instrument's resolution limitation. Nonetheless, the measured value fits very well to previously reported values for the viscosity of IPA at 20 °C.[56] The low viscosity combined with high wettability on cured MK surfaces was advantageous for the AM process, enabling both inks to spread over the previously printed MK absorber layer and to create a PhG template with micrometer-sized thickness.

To establish a printing window, it was necessary to gain further understanding of the curing process of the MK-absorber ink for which a time-resolved oscillation experiment was conducted at a constant frequency and amplitude within the LVE regime (1 Hz and 0.01% strain, respectively). The MK-absorber ink gradually increased in viscosity with the ongoing curing time (Figure 6C). The phase angle δ formed a peak only after 150 min, denoting the beginning of the formation of a cross-linked polymer network.[57] Up to this time point, the polymer should be technically extrudable. However, given the printing setup used and a pressure limit of 200 kPa, the MK-absorber ink could be continuously extruded for about 40 min, corresponding to a complex viscosity η^* of 3.8 kPa s. Longer printing times may be achievable through the application of higher extrusion pressures, although this was not a requirement in this study.

Building on previous findings, we printed a butterfly design with a pre-pyrolysis wingspan of 40 mm as an exemplary printed FGM-PhG sample. As shown in Figure 6E, the butterfly's perimeter was accurately reproduced, and sections printed with a single strut demonstrate that the MK-absorber layer sufficiently retained its shape, allowing the printing of curved geometries. However, some neighboring struts within the wings coalesced, which indicates a "printing resolution" limitation for this ink. Future improvements in flow behavior may be achieved by incorporating rheology modifiers,[58,59] having in mind the requirement that these should not interfere with the pyrolysis process or the color impression. Following the cure of the absorber layer, the PhG layer was printed on top of it using a particle concentration of 50 mg mL^{-1}. Lower concentrations resulted in a patchy final PhG layer, while higher concentrations did not significantly enhance the final color saturation and often led to needle clogging during printing.

The resultant FGM-PhG butterfly exhibited saturated blue structural coloration (Figure 6E) after heat treatment (Figure 1B), thus demonstrating the successful transition from the coating process to an AM process. This process, compared to previous work on AM of ceramic structural colors,[21] significantly reduces the required amount of monodisperse dispersion by employing a solid SiOC absorber layer and a μm-thin PhG layer. This translates into substantial cost savings and presents a novel, sustainable printing alternative for ceramic structural colors.

https://doi.org/10.1021/acsami.4c01047
ACS Appl. Mater. Interfaces 2024, 16, 22379–22390

High-Temperature Stability Study. To analyze the thermal stability of the FGM-PhG structural colors, starting samples with lower thickness were selected due to their macroscale crack-free appearance, albeit not having the brightest colors (see Figure 5C and accompanying discussion). The samples were heat-treated in an air atmosphere and exposed to different temperatures ranging from 800 to 1200 °C with varying dwell times ranging from 1 to 100 h (Figure 7).

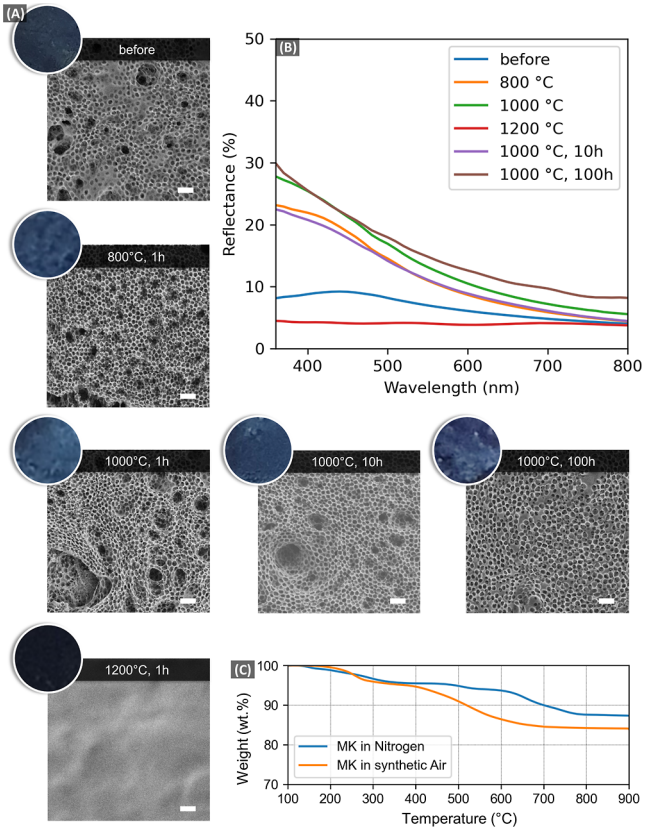

Figure 7. (A) Photographs and associated SEM images of FGM-PhG samples after exposure to various temperatures for different durations. Scale bars: 1 μm. (B) Reflectance spectra corresponding to each sample depicted in (A). (C) TGA profiles for MK heat-treated in nitrogen and synthetic air.

The samples heat-treated at 800 and 1000 °C retained their blue structural color (Figure 7A) with an additional improvement in their color saturation. This was associated with a significant increase in their reflectance (Figure 7B), attributed to the removal of the "free" turbostratic carbon at increased temperatures by the oxygen contained in the air atmosphere.[60] The turbostratic carbon is originally formed during pyrolysis in nitrogen, but remains unoxidized in the inert atmosphere.[16,60] This was additionally evidenced by a greater mass loss for MK-samples pyrolyzed in oxygen than in the samples pyrolyzed in nitrogen (Figure 7C): 15.9 wt % vs 12.7 wt %, respectively. The reduction of turbostratic carbon decreases the amount of absorbing moieties in the SiOC material and, thus, of the FGM-PhG structures, hence increasing their reflectance. Despite the oxidation of free carbon, the material is still clearly able to absorb light in the visible wavelength range, thereby sustaining the samples' structural coloration. Detrimental morphological changes in the microstructure of the photonic samples were not observed at these temperatures (Figure 7A). Conversely, upon increasing the temperature to 1200 °C, the samples clearly sintered with complete destruction of the 3D porous photonic structure, yet maintaining the absorber layer. Thereby, the samples heat-treated at this temperature consistently showed low reflectance of about 5% across the entire visible wavelength range.

To probe the influence of sustained heat exposure on the FGM-PhG, the samples were subjected to heating at 1000 °C for extended periods of 10 and 100 h. Remarkably, even after a 100 h exposure, no structural deformation or additional change in color or corresponding reflectance was observed. This indicates the high stability of the PDC-based FGM structural color provided that the temperature is kept below the 1200 °C limit. Compared with prior research presenting high-temperature stable structural colors, the thermal stability of the hereby developed PDC-based FGM-PhG structural color greatly exceeds those previously reported.[8,21,26] The reason for that lies on the fact that previous studies have focused on incorporating additional absorbers within the 3D photonic structure such as carbon black[21,26] or metal oxide nanoparticles.[8] Nonetheless, carbon black has been reported to oxidize at relatively low temperatures (~350 °C),[26] while metal oxide absorber particles that were added to a silica PhG structure could withstand a maximum temperature of 900 °C.[8] Our work demonstrates the advantages of adding an already relatively high-temperature stable material, SiOC, as an absorber material and using the 3D nanostructuring of the same PDC to generate color in an FGM approach. To the best of the authors' knowledge, the FGM-PhG structural color presented in this study is the most thermally stable ceramic structural color ever reported.

CONCLUSIONS

This study demonstrated for the first time that noniridescent structural colors can be produced from the highly absorbing ceramic SiOC material also known as "black glass" when 3D nanostructuring is introduced into the material system. To exploit the light absorbing material characteristics combined with the 3D structure reflective characteristics, the design concept of FGM-PhG was introduced, thereby producing PDC structural coloration with high color saturation even in front of white backgrounds with highly illuminated surroundings.

An investigation of the process−structure−property relationships was used to optimize the color impression. Colloidal-assembly was guided by dispersion medium modification, where the smaller surface tension of IPA prevented crystallization during dispersion medium evaporation, while assuring good wetting of the MK-based absorber layer. An optimal value was identified for the PhG feature size, above which single feature resonances dominate the 3D PhG reflectance behavior. Meanwhile, the optimal PhG layer height was identified as a trade-off between uniformity and color brightness. To showcase the exceptional processing flexibility of PDCs compared to traditional ceramics, the three-step coating process was converted into an AM process, proving that the discovered design requirements could be directly transferred to printed geometries. The excellent thermal stability of the SiOC ceramic material is preserved after the nanostructuring into 3D PhGs, which maintained their structural coloration even when exposed to 1000 °C for 100 h, greatly outperforming previously reported structures.

https://doi.org/10.1021/acsami.4c01047
ACS Appl. Mater. Interfaces 2024, 16, 22379−22390

METHODS

Preparation of Inks. In this study, two sample preparation strategies were employed: a three-step coating deposition method and AM. Both strategies utilized three types of inks to first create the absorber layer and then subsequently deposit the PMMA PhG template on top of it and infiltrate the PMMA PhG template with the preceramic polymer. Finally, the FGM-PhG samples were obtained via tailored pyrolysis (Figure 1A,B). For this study, SILRES MK (Wacker-Chemie GmbH, München, Germany), a commercial polymethylsiloxane, was used as the preceramic polymer.

For the absorber layer, 18.6 wt % of isopropyl alcohol (IPA) was added to MK (weight ratios are stated with respect to the amount of MK) based on an ink preparation protocol previously reported in literature.[17] To aid homogenization of the solution, the mixture was heated to 70 °C and stirred in an enclosed vial for at least 30 min. Once a homogeneous solution was formed, the vial was cooled to room temperature. Right before shaping (either via doctor blading or AM), 0.5 wt % of cross-linking agent (GF91, Wacker-Chemie GmbH, München, Germany) was added. For the PhG structure, aqueous PMMA dispersions (Microparticles GmbH, Berlin, Germany) were dried at room temperature to form loose particle agglomerates, which were subsequently redispersed in IPA and sonicated for at least 30 min in an ultrasonic bath. The dispersions in IPA were freshly prepared for each sample preparation to avoid significant swelling of the particles in the dispersion. Dispersions with varied particle concentrations (12.5, 20, 25, 50, and 100 mg mL^{-1}) and various average diameters (286, 406, and 499 nm) were prepared for the parameter studies (more details in the following section). At last, an infiltration solution with a MK concentration of 2.1−8.4 mg mL^{-1} was prepared in IPA and, right before infiltration, 2 wt % of the cross-linker GF91 was added to the solution. The concentrations were defined and varied based on an approximation of the required amount of MK to fill the pores in the PMMA PhG template (estimated packing fraction 0.64) as well as based on the amount of solution required to wet the entire PhG template.

Coating Deposition. All coating deposition steps were performed at room temperature and under ambient conditions; i.e., the choice of using MK as the preceramic polymer allowed us to fabricate samples without the need of a glovebox. To produce FGM-PhG samples, a bulk (nonporous) MK-layer was first deposited via doctor blading on Parafilm employing a MK−IPA solution (described in the previous section). Parafilm was used as the substrate material for sample preparation to allow easy sample removal once the sample was cured. Additionally, a stiff PLA sheet aided as a support to prevent deformation of the Parafilm during doctor blading (Figure 1A). To control the shape and thickness of the bulk MK-layer, custom thermoplastic polyurethane (TPU) molds produced via fused deposition modeling were used. The absorber layer was allowed to cure for at least 12 h at room temperature prior to PMMA PhG template deposition. The PMMA−IPA dispersions were deposited inside a second TPU ring that was placed on top of the first ring to allow spreading of the PMMA−IPA dispersions on the MK absorber layer, while constraining the area to the MK absorber layer surface (Figure 1A). By constraining the drop cast area with the second TPU ring, we could additionally control the structure thickness by simply varying the drop-cast volume. The cast volume and the particle concentration as well as the particle size were varied to study various process−structure−property relationships (see Supporting Information, Table S1). The dispensed PMMA−IPA dispersions were dried for 1 h. After drying, the PhG template was infiltrated with a MK solution. The concentration of MK was adjusted to the amount of deposited PMMA particles (see Supporting Information, Table S1). Additional samples were produced on sapphire substrates to investigate the optical properties without the first absorber layer and with PhG templates produced from aqueous PMMA dispersions. To improve wetting of the sapphire substrates, they were initially plasma cleaned (20 min exposure to an oxygen plasma; Polaron PT7160, Quorum Technologies), followed by heating at 80 °C on a hot plate. PTFE rings with a diameter of 20 mm were used to define the drop-cast area of 150 μL of aqueous PMMA dispersion at 20 mg mL^{-1} with various particle sizes (286, 406, and 499 nm). During drop-cast, the temperature was kept at 80 °C, thereby reducing evaporation time to improve homogeneity of the particle deposition.[61] After 1 h of drying time, infiltration was performed with 100 μL of 8.4 mg mL^{-1} MK solution in IPA at room temperature. All infiltrated samples were cured for 12 h at room temperature prior to pyrolysis.

Additive Manufacturing. After investigating and determining the design principles for the FGM-PhG samples via coating deposition, the three-step processing strategy was transferred to an AM process, namely, direct writing. Here, we used the extrusion-based BioX printer (CELLINK, Gothenburg, Sweden) equipped with a 3 mL cartridge pneumatic print head. For each aforementioned printing step and ink, different printing parameters were chosen based on the inks' rheology (discussed in the Results and Discussion section) and filament stability (Table 1).

Table 1. Printing Parameters for the Three Printing Steps and Inks[a]

ink	nozzle/needle	pressure (kPa)	printing speed (mm s^{-1})
MK in IPA type I	20 GA nozzle	80−130	5
PMMA in IPA	20 GA needle	2−4	5
MK in IPA type II	27 GA needle	2−4	5

[a]For a detailed description of the ink composition and preparation, please refer to Preparation of Inks.

To facilitate the cartridges' filling, they were filled with the heated (70 °C) MK solution and let cool down to room temperature prior to the absorber layer printing. After addition of the cross-linker, the cartridges were mixed in a planetary mixer (ARE 250, Thinky, Japan) twice for 1 min at 2000 rpm to homogeneously distribute the cross-linker inside the viscous MK solution. The absorber material was deposited on Parafilm in less than 30 min to avoid premature curing during printing and then cured for 12 h at room temperature prior to subsequent processing steps. For the printing of the PMMA PhG template on top of the absorber layer, PMMA−IPA dispersions with a concentration of 50 mg mL^{-1} and particle diameter of 406 ± 10 nm were utilized, while a 8.4 mg mL^{-1} MK−IPA solution with 2 wt % cross-linker was used for infiltration. The printed samples were cured for 12 h at room temperature prior to removal of the Parafilm and subsequent pyrolysis.

Heat Treatment. Following the sample preparation process, the FGM-PhG samples were heat-treated in a tube furnace under a nitrogen atmosphere for MK cross-linking, PMMA-template removal, and finally conversion via pyrolysis of the preceramic polymer into a SiOC-PDC (Figure 1B). The cycle parameters were selected based on a previously reported cycle developed by Colombo's group for samples containing the same preceramic polymer MK and also PMMA-template particles.[17] In the first segment of the heating cycle, the temperature was gradually increased from room temperature to 300 °C at a heating rate of 1 °C min^{-1}. The FGM-PhG samples were then allowed to dwell at 300 °C for 3 h to enable cross-linking while also removing the PMMA. Subsequently, the temperature was further raised to 1000 °C, where the samples were kept for 2 h. The cooling process was conducted inside the furnace at a cooling rate of 5 °C min^{-1}.

Characterization. Thermogravimetric analysis (TGA) was conducted on dried PMMA particles, cured MK, and their mixtures (STA449 F5, Netzsch Gerätebau GmbH). The samples were subjected to a heating ramp of 10 °C min^{-1} up to 1000 °C under a nitrogen atmosphere, enabling the study of the decomposition and pyrolysis process. DTG data were acquired from the derivative of the TGA data with respect to time. Rheological properties of the inks were determined by rotational rheometry (Kinexus Pro, Netzsch) at a constant temperature of 20 °C. The samples were presheared for 10 min at 100 s^{-1} to eliminate flow history, and 40 mm roughened parallel plates were used to minimize sample slippage during

https://doi.org/10.1021/acsami.4c01047
ACS Appl. Mater. Interfaces 2024, 16, 22379−22390

measurement. The gap size was set to 1 mm for MK-absorber ink and 0.2 mm for low viscous PMMA−IPA dispersion as well as MK−IPA infiltration ink. Contact angle measurements were performed with a custom-made droplet deposition device. Submillimeter-sized droplets were deposited on cured MK substrates using a 25 μL syringe (1702 RN, Hamilton Company) with a polytetrafluoroethylene-coated needle (inner-diameter of 0.127 mm, Hamilton Company). Side view monitoring of the deposited droplets was accomplished via a CMOS camera (EO-10012C 1/2″ CMOS, Edmund Optics) with a 5× optical magnification lens, positioned adjacent to the sample stage. Average contact angles were computed using ImageJ software, based on five repeats.

Microstructural analysis was performed by scanning electron microscopy (Zeiss Supra VP55) with an accelerating voltage of 1.5 kV at an average working distance of around 5 mm, while elemental information was acquired with 10 kV at a distance of 8 mm and the energy-dispersive X-ray spectroscopy module. X-ray diffraction (Bruker AXS D8 Advance, Cu Kα) analysis was used to characterize the phase formed after pyrolysis.

Optical properties, namely, diffuse reflectance spectra, was acquired in the visible wavelength range using a UV−vis−NIR spectrophotometer (Lambda 1050, PerkinElmer) equipped with an integrating sphere accessory. High-temperature annealing experiments were performed in a chamber furnace in an air atmosphere. The samples were heat-treated at 800, 1000, or 1200 °C for 1 h. Further longer dwell times of 5, 10, and 100 h were investigated at 1000 °C. The heating rate was set to 5 °C min^{-1}, while cooling was performed with a rate of 10 °C min^{-1}.

■ ASSOCIATED CONTENT

Supporting Information

The Supporting Information is available free of charge at https://pubs.acs.org/doi/10.1021/acsami.4c01047.

Details about solution and dispersion compositions used for sample preparation; cross-sectional images of sessile droplets utilized for contact angle analyses; EDX and XRD data for produced PDCs; SEM images for polyPhC structures produced with various PMMA-template sizes; results for the postprocessing via atomic layer deposition; photographs and SEM cross sections of FGM-PhG structures presenting whitening effect; and SEM cross sections of deposited PMMA PhG templates prior to MK infiltration (PDF)

■ AUTHOR INFORMATION

Corresponding Author

Kaline P. Furlan − *Hamburg University of Technology, Institute of Advanced Ceramics, Integrated Materials Systems Group, 21073 Hamburg, Germany;* orcid.org/0000-0003-4032-2795; Email: kaline.furlan@tuhh.de

Authors

Benedikt F. Winhard − *Hamburg University of Technology, Institute of Advanced Ceramics, Integrated Materials Systems Group, 21073 Hamburg, Germany*

Alberto Gomez-Gomez − *Hamburg University of Technology, Institute of Advanced Ceramics, Integrated Materials Systems Group, 21073 Hamburg, Germany*

Laura G. Maragno − *Hamburg University of Technology, Institute of Advanced Ceramics, Integrated Materials Systems Group, 21073 Hamburg, Germany*

Diego Ribas Gomes − *Hamburg University of Technology, Institute of Advanced Ceramics, Integrated Materials Systems Group, 21073 Hamburg, Germany;* orcid.org/0000-0003-4959-0032

Complete contact information is available at: https://pubs.acs.org/10.1021/acsami.4c01047

Notes

The authors declare no competing financial interest.

■ ACKNOWLEDGMENTS

The authors gratefully acknowledge the financial support from the Deutsche Forschungsgemeinschaft (DFG, German Research Foundation)-Projektnummer 192346071-SFB 986, project C4. We further thank Prof. Gerold A. Schneider and Prof. Manfred Eich for the laboratory infrastructure and equipment access. We also thank the students J. Katz and L. Carcone for their initial involvement in the preliminary experiments of this study.

■ REFERENCES

(1) Armstrong, E.; O'Dwyer, C. Artificial opal photonic crystals and inverse opal structures - fundamentals and applications from optics to energy storage. *J. Mater. Chem. C* **2015**, *3* (24), 6109−6143.

(2) Shang, G.; Eich, M.; Petrov, A. Photonic glass based structural color. *APL Photonics* **2020**, *5* (6), 060901.

(3) Herbst, W.; Hunger, K.; Wilker, G.; Ohleier, H.; Winter, R. *Industrial Organic Pigments*; Wiley, 2004..

(4) Shi, Y. F.; Meng, Y.; Chen, D. H.; Cheng, S. J.; Chen, P.; Yang, H. F.; Wan, Y.; Zhao, D. Y. Highly Ordered Mesoporous Silicon Carbide Ceramics with Large Surface Areas and High Stability. *Adv. Funct. Mater.* **2006**, *16* (4), 561−567.

(5) Sung, I.-K.; Christian; Mitchell, M.; Kim, D.-P.; Kenis, P. J. A. Tailored Macroporous SiCN and SiC Structures for High-Temperature Fuel Reforming. *Adv. Funct. Mater.* **2005**, *15* (8), 1336−1342.

(6) Wang, H.; Li, X.; Yu, J.-S.; Kim, D.-P. Fabrication and characterization of ordered macroporous PMS-derived SiC from a sacrificial template method. *J. Mater. Chem.* **2004**, *14* (9), 1383.

(7) Häntsch, Y.; Shang, G.; Petrov, A.; Eich, M.; Schneider, G. A. YSZ Hollow Sphere Photonic Glasses: Tailoring Optical Properties for Highly Saturated Non-Iridescent Structural Coloration. *Adv. Opt. Mater.* **2019**, *7* (18), 1900428.

(8) Yamanaka, T.; Tarutani, N.; Katagiri, K.; Inumaru, K.; Takeoka, Y.; Masui, T. High Heat Resistance of the Structural Coloration of Colloidal Arrays with Inorganic Black Additives. *ACS Appl. Mater. Interfaces* **2022**, *14* (25), 29324−29330.

(9) Vakifahmetoglu, C.; Zeydanli, D.; Colombo, P. Porous polymer derived ceramics. *Mater. Sci. Eng., R* **2016**, *106*, 1−30.

(10) Boehm, A. K.; Husmann, S.; Besch, M.; Janka, O.; Presser, V.; Gallei, M. Porous Mixed-Metal Oxide Li-Ion Battery Electrodes by Shear-Induced Co-assembly of Precursors and Tailored Polymer Particles. *ACS Appl. Mater. Interfaces* **2021**, *13* (51), 61166−61179.

(11) Hatton, B.; Mishchenko, L.; Davis, S.; Sandhage, K. H.; Aizenberg, J. Assembly of large-area, highly ordered, crack-free inverse opal films. *Proc. Natl. Acad. Sci. U.S.A.* **2010**, *107* (23), 10354−10359.

(12) Vasquez, Y.; Kolle, M.; Mishchenko, L.; Hatton, B. D.; Aizenberg, J. Three-Phase Co-assembly: In Situ Incorporation of Nanoparticles into Tunable, Highly Ordered, Porous Silica Films. *ACS Photonics* **2014**, *1* (1), 53−60.

(13) Vowinkel, S.; Schäfer, C. G.; Cherkashinin, G.; Fasel, C.; Roth, F.; Liu, N.; Dietz, C.; Ionescu, E.; Gallei, M. 3D-ordered carbon materials by melt-shear organization for tailor-made hybrid core-shell polymer particle architectures. *J. Mater. Chem. C* **2016**, *4* (18), 3976−3986.

(14) Vowinkel, S.; Boehm, A.; Schäfer, T.; Gutmann, T.; Ionescu, E.; Gallei, M. Preceramic core-shell particles for the preparation of hybrid colloidal crystal films by melt-shear organization and conversion into porous ceramics. *Mater. Des.* **2018**, *160*, 926−935.

(15) Vowinkel, S.; Malz, F.; Rode, K.; Gallei, M. Single-source macroporous hybrid materials by melt-shear organization of core-shell particles. *J. Mater. Sci.* **2017**, *52* (19), 11179−11190.

(16) Colombo, P.; Mera, G.; Riedel, R.; Sorarù, G. D. Polymer-Derived Ceramics: 40 Years of Research and Innovation in Advanced Ceramics. *J. Am. Ceram. Soc.* **2010**, *93*, 1805−1837.
(17) Huang, K.; Elsayed, H.; Franchin, G.; Colombo, P. 3D printing of polymer-derived SiOC with hierarchical and tunable porosity. *Addit. Manuf.* **2020**, *36*, 101549.
(18) Zhou, S.; Mei, H.; Chang, P.; Lu, M.; Cheng, L. Molecule editable 3D printed polymer-derived ceramics. *Coord. Chem. Rev.* **2020**, *422*, 213486.
(19) Zhang, Z.; Wang, C.; Wang, Q.; Zhao, Y.; Shang, L. Cholesteric cellulose liquid crystal ink for three-dimensional structural coloration. *Proc. Natl. Acad. Sci. U.S.A.* **2022**, *119* (23), No. e2204113119.
(20) Boyle, B. M.; French, T. A.; Pearson, R. M.; McCarthy, B. G.; Miyake, G. M. Structural Color for Additive Manufacturing: 3D-Printed Photonic Crystals from Block Copolymers. *ACS Nano* **2017**, *11* (3), 3052−3058.
(21) Demirörs, A. F.; Poloni, E.; Chiesa, M.; Bargardi, F. L.; Binelli, M. R.; Woigk, W.; de Castro, L. D. C.; Kleger, N.; Coulter, F. B.; Sicher, A.; Galinski, H.; Scheffold, F.; Studart, A. R. Three-dimensional printing of photonic colloidal glasses into objects with isotropic structural color. *Nat. Commun.* **2022**, *13* (1), 4397.
(22) Llorens, J. S.; Barbera, L.; Demirörs, A. F.; Studart, A. R. Light-Based 3D Printing of Complex-Shaped Photonic Colloidal Glasses. *Adv. Mater.* **2023**, *35*, No. e2302868.
(23) Zhou, J.; Li, H.; Ye, L.; Liu, J.; Wang, J.; Zhao, T.; Jiang, L.; Song, Y. Facile Fabrication of Tough SiC Inverse Opal Photonic Crystals. *J. Phys. Chem. C* **2010**, *114* (50), 22303−22308.
(24) García, P.; Sapienza, R.; Blanco, Á.; López, C. Photonic Glass: A Novel Random Material for Light. *Adv. Mater.* **2007**, *19* (18), 2597−2602.
(25) García, P. D.; Sapienza, R.; López, C. Photonic glasses: a step beyond white paint. *Adv. Mater.* **2010**, *22* (1), 12−19.
(26) Nakamae, K.; Hano, N.; Ihara, H.; Takafuji, M. Thermally stable high-contrast iridescent structural colours from silica colloidal crystals doped with monodisperse spherical black carbon particles. *Mater. Adv.* **2021**, *2* (18), 5935−5941.
(27) Bik, M.; Stygar, M.; Jeleń, P.; Dąbrowa, J.; Leśniak, M.; Brylewski, T.; Sitarz, M. Protective-conducting coatings based on black glasses (SiOC) for application in Solid Oxide Fuel Cells. *Int. J. Hydrogen Energy* **2017**, *42* (44), 27298−27307.
(28) Guo, A.; Roso, M.; Modesti, M.; Liu, J.; Colombo, P. Preceramic polymer-derived SiOC fibers by electrospinning. *J. Appl. Polym. Sci.* **2014**, *131*, 39836, .
(29) Kaspar, J.; Terzioglu, C.; Ionescu, E.; Graczyk-Zajac, M.; Hapis, S.; Kleebe, H.-J.; Riedel, R. Stable SiOC/Sn Nanocomposite Anodes for Lithium-Ion Batteries with Outstanding Cycling Stability. *Adv. Funct. Mater.* **2014**, *24* (26), 4097−4104.
(30) Yan, Q.; Gao, L.; Sharma, V.; Chiang, Y.-M.; Wong, C. C. Particle and substrate charge effects on colloidal self-assembly in a sessile drop. *Langmuir* **2008**, *24* (20), 11518−11522.
(31) Gast, A. P.; Russel, W. B. Simple Ordering in Complex Fluids. *Phys. Today* **1998**, *51* (12), 24−30.
(32) Häntsch, Y.; Shang, G.; Lei, B.; Winhard, B.; Petrov, A.; Eich, M.; Holm, E.; Schneider, G. A.; Furlan, K. P. Tailoring Disorder and Quality of Photonic Glass Templates for Structural Coloration by Particle Charge Interactions. *ACS Appl. Mater. Interfaces* **2021**, *13* (17), 20511−20523.
(33) James, G. *Lange's Handbook of Chemistry, Sixteenth Edition, 70th Anniversary Edition; McGraw-Hill Standard Handbooks*; McGraw-Hill, 2005.
(34) Kralchevsky, P. A.; Nagayama, K. Capillary forces between colloidal particles. *Langmuir* **1994**, *10* (1), 23−36.
(35) Dicuangco, M.; Dash, S.; Weibel, J. A.; Garimella, S. V. Effect of superhydrophobic surface morphology on evaporative deposition patterns. *Appl. Phys. Lett.* **2014**, *104* (20), 201604.
(36) Xia, T.; Luo, W.; Hu, F.; Qiu, W.; Zhang, Z.; Lin, Y.; Liu, X. Y. Fabrication of Crack-Free Photonic Crystal Films on Superhydrophobic Nanopin Surface. *ACS Appl. Mater. Interfaces* **2017**, *9* (26), 22037−22041.
(37) Valandro, S. R.; Lombardo, P. C.; Poli, A. L.; Horn Jr, M. A.; Neumann, M. G.; Cavalheiro, C. C. S. Thermal properties of poly (methyl methacrylate)/organomodified montmorillonite nanocomposites obtained by in situ photopolymerization. *Mater. Res.* **2013**, *17* (1), 265−270.
(38) Kashiwagi, T.; Hirata, T.; Brown, J. E. Thermal and oxidative degradation of poly(methyl methacrylate) molecular weight. *Macromolecules* **1985**, *18* (2), 131−138.
(39) Schneider, O. Thermoanalytical investigations on curing and decomposition of methyl silicone resin. *Thermochim. Acta* **1988**, *134*, 269−274.
(40) Fateh, T.; Richard, F.; Rogaume, T.; Joseph, P. Experimental and modelling studies on the kinetics and mechanisms of thermal degradation of polymethyl methacrylate in nitrogen and air. *J. Anal. Appl. Pyrolysis* **2016**, *120*, 423−433.
(41) Patel, B. B.; Walsh, D. J.; Kim, D. H.; Kwok, J.; Lee, B.; Guironnet, D.; Diao, Y. Tunable structural color of bottlebrush block copolymers through direct-write 3D printing from solution. *Sci. Adv.* **2020**, *6* (24), No. eaaz7202.
(42) Forster, J. D.; Noh, H.; Liew, S. F.; Saranathan, V.; Schreck, C. F.; Yang, L.; Park, J.-G.; Prum, R. O.; Mochrie, S. G. J.; O'Hern, C. S.; Cao, H.; Dufresne, E. R. Biomimetic isotropic nanostructures for structural coloration. *Adv. Mater.* **2010**, *22* (26−27), 2939−2944.
(43) Takeoka, Y.; Yoshioka, S.; Takano, A.; Arai, S.; Nueangnoraj, K.; Nishihara, H.; Teshima, M.; Ohtsuka, Y.; Seki, T. Production of colored pigments with amorphous arrays of black and white colloidal particles. *Angew. Chem., Int. Ed. Engl.* **2013**, *52* (28), 7261−7265.
(44) Teshima, M.; Seki, T.; Kawano, R.; Takeuchi, S.; Yoshioka, S.; Takeoka, Y. Preparation of structurally colored, monodisperse spherical assemblies composed of black and white colloidal particles using a micro-flow-focusing device. *J. Mater. Chem. C* **2015**, *3* (4), 769−777.
(45) Zhang, Y.; Dong, B.; Chen, A.; Liu, X.; Shi, L.; Zi, J. Using Cuttlefish Ink as an Additive to Produce Non-iridescent Structural Colors of High Color Visibility. *Adv. Mater.* **2015**, *27* (32), 4719−4724.
(46) Zhang, Y.; Han, P.; Zhou, H.; Wu, N.; Wei, Y.; Yao, X.; Zhou, J.; Song, Y. Highly Brilliant Noniridescent Structural Colors Enabled by Graphene Nanosheets Containing Graphene Quantum Dots. *Adv. Funct. Mater.* **2018**, *28* (29), 1802585.
(47) Zhao, T. H.; Jacucci, G.; Chen, X.; Song, D.-P.; Vignolini, S.; Parker, R. M. Angular-Independent Photonic Pigments via the Controlled Micellization of Amphiphilic Bottlebrush Block Copolymers. *Adv. Mater.* **2020**, *32* (47), No. e2002681.
(48) Li, Z.; Ma, T.; Li, S.; Gu, W.; Lu, L.; Yang, H.; Dai, Y.; Wang, R. High-Efficiency, Mass-Producible, and Colored Solar Photovoltaics Enabled by Self-Assembled Photonic Glass. *ACS Nano* **2022**, *16* (7), 11473−11482.
(49) Magkiriadou, S.; Park, J.-G.; Kim, Y.-S.; Manoharan, V. N. Absence of red structural color in photonic glasses, bird feathers, and certain beetles. *Phys. Rev. E: Stat., Nonlinear, Soft Matter Phys.* **2014**, *90* (6), 062302.
(50) Ohnuki, R.; Sakai, M.; Takeoka, Y.; Yoshioka, S. Optical Characterization of the Photonic Ball as a Structurally Colored Pigment. *Langmuir* **2020**, *36* (20), 5579−5587.
(51) Gallis, S.; Nikas, V.; Kaloyeros, A. E. Silicon Oxycarbide Thin films and Nanostructures: Synthesis, Properties and Applications. In *Modern Technologies for Creating the Thin-film Systems and Coatings*; Nikitenkov, N. N., Ed.; InTech, 2017.
(52) Kim, S.-H.; Magkiriadou, S.; Rhee, D. K.; Lee, D. S.; Yoo, P. J.; Manoharan, V. N.; Yi, G.-R. Inverse Photonic Glasses by Packing Bidisperse Hollow Microspheres with Uniform Cores. *ACS Appl. Mater. Interfaces* **2017**, *9* (28), 24155−24160.
(53) Chiu, R. C.; Garino, T. J.; Cima, M. J. Drying of Granular Ceramic Films: I, Effect of Processing Variables on Cracking Behavior. *J. Am. Ceram. Soc.* **1993**, *76* (9), 2257−2264.
(54) Singh, K. B.; Tirumkudulu, M. S. Cracking in drying colloidal films. *Phys. Rev. Lett.* **2007**, *98* (21), 218302.

https://doi.org/10.1021/acsami.4c01047
ACS Appl. Mater. Interfaces 2024, 16, 22379−22390

(55) Gibson, I.; Rosen, D.; Stucker, B.; Khorasani, M. *Additive Manufacturing Technologies*; Springer International Publishing, 2021.
(56) Brey, W. S. Analysis Data for Ternary System Isopropyl Alcohol-Isopropyl Ether-Water. *Anal. Chem.* **1954**, *26* (5), 838−842.
(57) Khimi, S. R.; Pickering, K. L. A new method to predict optimum cure time of rubber compound using dynamic mechanical analysis. *J. Appl. Polym. Sci.* **2014**, *131*, 40008.
(58) Lewis, J. A. Direct-write assembly of ceramics from colloidal inks. *Curr. Opin. Solid State Mater. Sci.* **2002**, *6* (3), 245−250.
(59) Smay, J. E.; Cesarano, J.; Lewis, J. A. Colloidal Inks for Directed Assembly of 3-D Periodic Structures. *Langmuir* **2002**, *18* (14), 5429−5437.
(60) Lu, K.; Erb, D.; Liu, M. Thermal stability and electrical conductivity of carbon-enriched silicon oxycarbide. *J. Mater. Chem. C* **2016**, *4* (9), 1829−1837.
(61) Li, Y.; Yang, Q.; Li, M.; Song, Y. Rate-dependent interface capture beyond the coffee-ring effect. *Sci. Rep.* **2016**, *6*, 24628.

https://doi.org/10.1021/acsami.4c01047
ACS Appl. Mater. Interfaces 2024, 16, 22379−22390